RSC Advances

ROYAL SOCIETY OF CHEMISTRY

www.rsc.org/advances

Computational and Experimental Studies on the Effect of Hydrogenation of Ni-doped TiO_2 Anatase Nanoparticles for the Application of Water Splitting

Chung-Ching Chuang, Cheng-Kuo Lin, T. T. Wang, V. Srinivasadesikan, P. Raghunath and M. C. Lin*

Center for Interdisciplinary Molecular Science, Department of Applied Chemistry, National Chiao Tung University, Hsinchu, Taiwan 300.

Abstract:

We have studied theoretically and experimentally the effect of Ni-doping in TiO_2 nanoparticles (NPs) on hydrogenation. The doped NPs can be hydrogenated readily in a much shorter time at T<623K under near atmospheric H_2 pressure. The hydrogenated black NP films exhibit a broad UV-Vis absorption extending well beyond 800 nm. The experimental data can be corroborated by quantum calculations. The barriers for dissociative adsorption of H_2 at the Ni and O_{2c} sites on the 2Ni-doped TiO_2 surface are significantly reduced from 48 kcal/mol on the undoped surface to 17 and 12 kcal/mol, respectively. The computed densities of states of the doped TiO_2 also show new absorption peaks in the band-gaps of the hydrogenated systems which exhibit a high efficiency of solar water-splitting over those of non-hydrogenated samples based on our preliminary study. The theoretical result also indicates that Ni-doping significantly affects the enthalpies of hydrogenation for formation of 2HO(b) and H_2O(b) in the bulk from 7 and 19 kcal/mol in the undoped TiO_2 to -76 and -69 kcal/mol in the 2Ni-TiO_2 system, respectively, with >80 kcal/mol increase in exothermicities.

***Corresponding author: chemmcl@emory.edu**

Introduction

Hydrogenation of TiO_2 nanoparticles (NPs) has been shown to significantly enhance the efficiency of water splitting in the visible region of the solar spectrum by photo-catalysis.[1-6] Chen *et al.*[3] carried out the hydrogenation of TiO_2 white powders at 473 K under 20 atm of H_2 for 5 days which blackened the TiO_2 powders due to surface disordering with about 0.3wt% of H_2 incorporation. The hydrogenated TiO_2 NPs enhanced the water splitting efficiency over those of pure TiO_2 by more than 2 orders of magnitude [4,5] with a high durability using methanol as a sacrificial agent. A similar study [4] on the hydrogenation of TiO_2 rutile nanowires (NWs) and anatase nanotubes (NTs) at 673K under H_2 atmosphere was found to improve the performance of photo-electrochemical water splitting with 200% enhancement in photocurrent and improvement in electrical conductivity and charge transportation, which were attributed to the formation of O-vacancies in TiO_2 with enhanced UV/visible and IR absorptions. Similar surface modifications have been accomplished by Zheng *et al.*[5] with the hydrogenation of protonated TiO_2 NTs in a 5% H_2 diluted in N_2 using a quartz flow tube at 773 K; the hydrogenated anatase consisted of microspheres of TiO_2 NWs with enhanced photo-catalytic activities. Sun and co-workers [7] studied the hydrogenation of well-defined nanocrystals of anatase TiO_2 at 723 K under 7 atm H_2 pressure; they reached as much as 1.4wt% of H-incorporation under a mild H_2 pressure at a rather high temperature condition. Interestingly, the results of their XRD, TEM, and Raman spectral measurements revealed no detectable morphological and crystallographic changes by hydrogenation, contrary to the finding of Chen *et al.*,[3] who ascribed the enhanced photo-catalytic effect to surface disordering. The nature and locations of the disordered black TiO_2 NPs have been studied in detail by Naldoni *et al.*[8] who characterized the blackened samples by different surface and optical measurements to understand the band-gap narrowing mechanism. The mechanism for

TiO_2 hydrogenation by H_2 dissociation and migration into its subsurface has been investigated computationally by Raghunath *et al.*[9] The controlling step for the hydrogenation process was reported to be the dissociative adsorption of H_2 on the TiO_2 surface with 47.8 kcal/mol energy barrier, to be followed by H-atom migration into the bulk with 27.8 kcal/mol barrier. In addition, H_2 was also found to be able to migrate molecularly into TiO_2 subsurface layers with 46.2 kcal/mol of barrier, which is competitive with the dissociative adsorption process. Most interestingly, both H and H_2 inside the cages of the crystal bulk can readily form HO-bonds, whose transformation into H_2O inside the bulk helps create O-vacancies and may result in the disordering of the surface layers as found experimentally. These theoretical results help explain the need of high temperature and high H_2 pressure for the hydrogenation process and provide a reasonable mechanism for the surface disordering process.

In this work, we have carried out an experimental study on the effect of Ni-doping in TiO_2 NPs with different amounts of the dopant on the hydrogenation process and investigated the optical properties of the doped NPs with and without hydrogenation. In addition we studied computationally the effect of Ni-doping on the hydrogenation process by comparing the barriers for H_2 dissociation and H-atom migration into the TiO_2 subsurface with and without doping. Ni is well known for its efficacy in dissociating the H_2 molecule; for example, Ni-oxide has been employed as the key catalyst in the anode of the LSM/Ni-YSZ solid oxide fuel cell system.[10-13] The mechanism for H_2 dissociation and H-atom migration in the Ni-YSZ anode has been studied by Weng *et al.*[12a] The results of our experimental finding on Ni-doping and its influence on hydrogenation and the quantum-mechanical calculations for H_2 dissociation, H-atom migration and band-gap properties for the Ni-doped TiO_2 are reported herein.

Experimental section

Synthesis of TiO_2 Nanoparticles: All the reagent grade chemicals were used directly without further purification. Nickel nitrate was employed as the Ni source in the synthesis of TiO_2 NPs by sol gel hydrothermal process. A desired amount of titanium isopropoxide in *i*-propanol solution was dropped into acetic acid aqueous solution mixed with a varying amount of $Ni(NO_3)_2$ powders. After stirring at 353K for 5hrs, the final mixture was sealed in a Teflon container throughout 12hrs of hydrothermal process at 593K. The acid residues were removed by filtrating and washing for several times using de-ionic water and ethanol. After being dried at 423K for 12hrs, the Ni-doped TiO_2 NPs with approximately 20 nm in diameters were obtained. In Figure 1(A), the Ni-doped TiO_2 NP powders are presented; their nominal weight ratios of Ni to Ti (Ni/Ti) are 1, 3.4, 5.0 and 7.5%. From the Figure 2, one can see that the color of Ni-doped TiO_2 NP powders gradually changes from pale yellow to bright yellow with increasing Ni concentration.

Results and discussions

Characterization of TiO_2 NPs with doping and hydrogenation: The thin films of TiO_2 NPs for UV-Vis analysis were made by dissolving the powders in ethanol and DI water solution and spin-coating the mixture at 1000 rpm. UV-Vis absorption spectra of Ni-TiO_2 substrates are presented in Figure 1 (B). All Ni-doped samples show clear red-shifted tails around 400 to 500 nm with respect to TiO_2 blank. The $Eg=1239.8/\lambda$ relation was used to estimate the energy gap by extrapolating the onset to the related baseline.[14] A significant absorption threshold band edge change from 3.25 (TiO_2) to 2.96 eV (5.0% Ni/TiO_2) is observed as shown in Table 1. A slight blue shift is also noted with the 7.5% Ni-TiO_2 NP sample. In Figure S1 we have also shown a similar set of UV-Vis absorption spectra detected by diffuse reflection

employing powders instead of thin-films, comparing those from 0.5%- and 5%-Ni-doped TiO_2 NPs with those of pure and hydrogenated TiO_2.

To further reduce the TiO_2 band-gap and increase the photo-absorption efficiency in the visible range, hydrogenation of the Ni-doped TiO_2 NPs has been performed and tested. In a homemade glass tube furnace, the yellow Ni-doped TiO_2 NP powders were placed in an open stainless boat. The hydrogenation process was carried out at 573 K for 3hr under 780 Torr H_2 gas. After the reaction, the color of Ni-doped TiO_2 powders changed dramatically as shown in Figure 2 (A). The system as well as the complete procedure of hydrogenation is presented in the Supplementary Information section.[15] The color varies from pale grey to dark grey with increasing Ni contents. The UV-Vis absorption spectra of the hydrogenated samples are presented in Figure 2 (B) which shows a pronounced enhancement in the absorption spectra throughout the entire visible range. Under the same hydrogenation condition, the white color of the undoped TiO_2 powder remains unchanged after the treatment. In Figure 1(B), the pale yellow powders (1% Ni) changes to light grey and the more concentrated Ni-TiO_2 powders (7.5% Ni) changes to black while the undoped TiO_2 powders remain white. This result indicates that Ni-doping significantly enhances the hydrogenation process and helps reduce the TiO_2 band-gap as supported by the results of the quantum-chemical calculation presented below. Our preliminary testing using the 0.5% and 5% Ni-doped TiO_2 NPs with 10% ethanol as sacrificial agent also show a significant enhancement in its water-splitting efficiency over those of non-hydrogenated TiO_2 with or without Ni-doping. Figure 3 shows the measured hydrogen evolution data obtained from the photo-catalytic dissociation of water irradiated with about 2 W power from a 1 kW Xe lamp; the result gives the relative efficiencies for the pure TiO_2, hydrogenated TiO_2, 5%Ni-doped TiO_2 and hydrogenated 5%Ni-doped TiO_2, 1 : 1 : 4 : 18. Table S1 in the Supplementary

Information[15] presents the corresponding H_2 evolution rate in units of mmole.g^{-1}.hr^{-1}.

Computational study

The adsorption and dissociation of H_2 on Ni-doped TiO_2(101) surface by the first-principles calculations were carried out with the Vienna ab initio simulation package (VASP)[16] using the DFT+U method.[17] For the total energy prediction, the exchange-correlation function treated by the generalized gradient approximation (GGA) with the Perdew-Burke-Ernzerhof formulation (PBE)[18] has been applied with spin-polarization throughout the system. Twenty four [TiO_2] units doped with one and two Ni atoms were modeled by (2×2×3) supercell slabs separated perpendicularly by a 15.0 Å vacuum space. The predicted lattice constants at the PBE level for the anatase crystal bulk are a=3.828Å and c= 9.677Å, in good agreement with the experimental values of a= 3.782 Å and c= 9.502 Å.[19] In our calculation, the surface area of the anatase (101) surface was 11.097 Å x 7.655 Å extended along the $\mathbf{<\bar{1}11>}$ and $\mathbf{<010>}$ direction. A 2×3×1 Monkhorst-Pack k-point sampling was used in the calculations. The predicted structure is presented in Figure S2 of the Supplementary Information.[15] To locate the transition states of the dissociative adsorption the climbing-image nudged-elastic band (CINEB) method was applied.[20] To correct the strong on-site Coulomb repulsion of Ti and Ni 3d states, the value of U was taken to be 4 eV, consistent with that employed in previous reports.[9,21,22]

H_2 adsorption and dissociation on Ni-doped TiO_2 (101): We have investigated the molecular adsorption and dissociative adsorption of H_2 on the 1 and 2 Ni-doped anatase surfaces, denoted by 1Ni-TiO_2 and 2Ni-TiO_2, respectively. In the absence of a dopant four sites have been identified on the TiO_2 surface as labeled in Figure S2. Among the four, there are 2 active sites on the surface which may interact with molecular hydrogen; these are five-fold coordinated titanium (Ti_{5c}) and twofold bridging oxygen (O_{2c}). The remaining two sites are three-fold coordinated oxygen

(O_{3c}) and six-fold coordinated titanium (Ti_{6c}); they are not active as the other two. In the 1-Ni doped case, one Ni atom replaces one of the Ti_{5c} atoms on the surface, labeled as D1, and in the 2-Ni doped case 1 Ni substitutes a Ti_{5c} on the surface, also labeled as D1, and the other Ni atom replaces a Ti_{6c} atom inside the bulk which is labeled as D2 (see Figure S2). In terms of the Ni concentration, the Ni/Ti ratio in the 1- and 2-Ni doped TiO_2 is approximately equivalent to the experimental concentration of 4 and 8 %, respectively.

The interaction of H_2 with clean and doped TiO_2 surfaces was found to be rather weak; on the undoped surface H_2 can physisorb on an O_{2c} site with 0.3 kcal/mol binding energy[9], whereas on the Ni-doped surface the interaction becomes weakly repulsive at both Ni and O_{2c} sites. A Bader charge analysis gives small net charges of ~0.02 *e* to the H_2 on the 1Ni-TiO_2 and 2Ni-TiO_2 surface giving rise to the small repulsive energy as shown in Table S2. For the dissociative adsorption of H_2, on the other hand, the barriers for H_2 dissociation at the Ni- and O_{2c} sites of the 1Ni-TiO_2 surface are predicted to be significantly reduced to as low as 12.1 and 6.1 kcal/mol, respectively, from that on the undoped TiO_2 surface, 47.8 kcal/mol[9] (see Figure S3(a) and (b). Most notably, the predicted enthalpy changes for the dissociative adsorption processes producing H-O_{3c},H-O_{2c}-1Ni-TiO_2(a) and 2H-O_{2c}-1Ni-TiO_2(a) from the initial interaction on the Ni and O_{2c} sites are significantly greater than that on the undoped surface, ΔH = - 18.3 kcal/mol producing 2H-O_{2c}-TiO_2(a)[9], by as much as -77 and -80 kcal/mol, respectively, as shown in Figures S3(a) and (b). The dissociative adsorption energy barriers, 17.4 and 12.4 kcal/mol on the Ni and O_{2c} sites, respectively, on the 2Ni-TiO_2 surface are depicted in Figures S3(c) and (d). The corresponding geometries are shown in Figures S4 and S5. For the dissociative adsorption on the latter, more reactive O_{2c} site, its detailed PES including the H_2 dissociation on the surface, H-atom migration into the bulk and the ultimate H_2O

formation inside the bulk, to be discussed below, is presented in Figure 4 for comparison with the analogous steps predicted for the undoped TiO_2 surface[9]. The corresponding geometries of H_2 dissociation and migration on undpoed TiO_2 are shown in Figure S6. The energetics for the key intermediates, transition states and products of these two systems are also summarized in Table S2 for a closer examination. *The most significant finding revealed by the theoretical calculation for the initial dissociative adsorption of H_2 on the Ni-doped TiO_2 surface is the enormous catalytic effect of Ni on the reduction of the H_2-dissociation barriers and the very large exothermicities associated with the formation of surface hydroxyl species* (2 HO_{2c}(a) (i.e., 2H-O_{2c}-2Ni-TiO_2(a)) or the mixed HO_{2c}(a) and HO_{3c}(a), H-O_{3c}-2Ni-TiO_2(a)). It should also be mentioned that on account of the considerably lower barriers for the dissociative adsorption processes, our extensive searches for the direct H_2-molecular migration from the 1Ni- or 2Ni-TiO_2 surface into its subsurface failed to locate its transition state (which was found to be 46.2 kcal/mol for the undoped surface[9] as alluded to in the Introduction); the searches always converged to those of the dissociative adsorption processes. This is also an interesting finding which evidently suggests that the hydrogenation of the Ni-doped TiO_2 NPs occurs exclusively by H-atom formation and diffusion reactions on the surface and inside the bulk of the systems as discussed below.

H-atom migration: In the undoped anatase system[9], the migration of the H atoms into the bulk played a key role in the hydrogenation of TiO_2 NPs which led to enhanced water-splitting efficiencies.[4,5,23] The barrier for H-migration into a subsurface layer was predicted to be 26.4 kcal/mol.[9] We have investigated the effect of Ni-doping on the migration of an H atom adsorbed on the surface, HO_{2c}(a), into the bulk and compared the transition state barriers for each step along the migration path: HO_{2c}(a) → HO_{3c}(a) → H_{BD1}(b) → H_{BD2}(b), where H_{BD1}(b) and H_{BD2}(b) denote the H atom

undergoes bulk diffusion to site 1 and site 2, respectively (see Figures S3(e), (f) and S7 and Table S3). Interestingly, the barriers for H-migration into the bulk for the doped and undoped[9] systems are very similar to each other, suggesting that in the 1Ni-doped case, the migration kinetics should be quite similar. Notably, the full PESs for the migration of H atoms after the dissociative adsorption of H_2(g) on the undoped and doped 2Ni-TiO_2 surfaces, up to the formation of H_2O inside the bulk as shown in Figure 4, are also very similar in their barrier heights for the individual steps along their reaction paths. The major differences, again, lie in the initial dissociative adsorption barriers and the overall exothermicities for the formation of $2HO_{2c}$(a) on the surface, and 2HO(b) and H_2O(b) inside the bulk; for the latter two products, the enthalpy differences without and with doping are as much as -83.6 and -87.7 kcal/mol, revealing a much greater stability of hydrogen inside the bulk of TiO_2 with Ni-doping.

DOS of H_2 and H in Ni-doped TiO_2: To corroborate the experimental observation of UV-Vis spectra of hydrogenated Ni-doped TiO_2 NPs, we have investigated further to understand the Ni effect on band-gap reduction by incorporation of hydrogen. The density of states (DOS) and projected DOS (PDOS) on the Ni-doped TiO_2 surface are calculated by using the DFT + U method with the value of U = 4 eV for Ti and Ni as mentioned before. The results are presented in Figure 5; panel (5a) shows the DOS of undoped TiO_2 (101). The top of the valence band (VB) mainly consisting of the 2p states of oxygen was found to lie within 4.5 and 0 eV with the domination of Ti 3d states at the lower part of the conduction band (CB), consistent with previous reports.[9,24] The calculated DOS for the 2Ni-doped TiO_2 is shown in panel (5b) which indicates that the band gap is reduced to 2.79 eV (cf. the predicted undoped TiO_2, 2.90 eV). Here, we observe new localized states appearing between VB and CB at 1.23 eV above the VB. These new peaks in the band gap of the Ni-doped TiO_2 derive mainly from the 3d states of Ni and 2p states of O with a minor contribution from Ti.

Also, our experimental results show the band-gap reduction from 3.26 eV for TiO_2 to 2.98 eV for 5% Ni doped TiO_2 (see Table 1). In panel (5c) for an H atom adsorbed on an O_{2c} site and another H bonding with an O in the sublayer, giving H-O_{sub2},H-O_{2c}-2Ni(a), the Fermi level is located at the 0.2 eV above the VB and the band gap is reduced by 0.2 eV compared to the un-doped TiO_2. The DOS indicates that the impurity states produced the minor peaks near the top edge of the VB mostly contributed by Ni and O. However, two new prominent localized peaks appear at 0.7~ 1.0 eV above the Fermi level; the PDOS of the Ni, O and H shows that the new states result mostly from Ni3d and O2p orbitals with a negligible contribution from the H atoms. To further elucidate the role of the H atom on the surface *vs* that inside the bulk, we have carried out the DOS calculations independently for an H atom on the surface attached to O_{2c} and in the bulk attached to O_{sub3}; the results shown in Figure S8 indicate that new impurity peaks appear at 1.0 eV and 1.5 eV, respectively, above the Fermi level and the band gaps have been reduced by ~0.2 eV compared to that of the undoped TiO_2. In the H-O_{sub3}-2Ni(b) case, another new peak appears at 0.3 eV above the VB. The result of the DOS calculation for 2H atoms inside the bulk of the 2Ni-doped TiO_2, 2HO-2Ni(b), is shown in panel (5d). The two H atoms get incorporated interstitially producing two OH groups at the O_{sub1} and O_{sub3} sites. In this case, the Fermi level appears at ~0.5 eV above the VB and the band gap is reduced to 2.80 eV (c.f. the anatase gap 2.90 eV). The two new impurity peaks appearing at the edge of the VB lying below the Fermi level at ~ 0.2 and 0.06 eV, may be attributed to a stronger interaction between the Ni 3d and O 2p orbitals. Also, another new peak appears at 0.7 eV above the Fermi level may be attributed to Ni 3d and O 2p orbitals. As shown in panel (5e), we have also calculated the DOS for the H_2O formed in the subsurface of the 2Ni-TiO_2 system. Two new localized states appear at 0.7 and 1.5 eV above the VB. The band gap has been reduced to 2.64 eV (c.f. 2.90 eV for clean TiO_2

and 2.78 eV for 2Ni-TiO_2). The band gap reduction with the two new localized states appearing between the VB and CB derive mainly from the Ni and its neighboring O atoms with a negligible contribution from Ti3d.

In order to understand the reduction process in the Ni-doped TiO_2 system, we have carried out Bader charge analyses using the DFT + U method as shown in Figure S9. According to the analysis, the charge of O and Ti atoms in the undoped TiO_2 are –0.92*e* and 2.01*e,* respectively, where *e* is the magnitude of the charge on an electron (see Figure S9(a)). In the 2-Ni doped case, Ni (at the D1 site) bonding with one of the neighboring O_{2c} oxygens, the charge of the oxygen is predicted to be -0.69 *e*, changing noticeably from -0.92 *e* in the clean TiO_2 surface. The charge of the Ni(D1) is 1.37*e* and that of the O_{3c} on the surface is ~ -0.96 *e*. The bond length between Ni and O at the O_{2c} site is observed to be shortened to 1.793 Å, comparing with other Ni-O_{3c} bonds, 1.924 Å. The charge of the second Ni located in the subsurface is predicted to be 1.38*e*. The charges of surrounding oxygens around Ni are noted to be reduced by 0.1*e* ~ 0.28*e* comparing with that in the clean TiO_2 (Figure S9(b)). In the H_2 adsorption on the surface, as shown in Figures S9(c) and (d), there is a negligible charge transfer between the H_2 and the surface of the Ni-doped TiO_2. After the H_2 dissociative adsorption at an O_{2c} site of the 2Ni-TiO_2 surface producing 2H-O_{2c}-2Ni-TiO_2(a), the charge of the O atom is predicted to be -1.20*e* (see Figure S9e), a significant change from -0.69*e* cited above. It is noteworthy that the charge of the other neighboring O_{2c} is also observed to be increased by -0.3*e* from that in 2Ni-TiO_2. The bond length between Ni and the O_{2c} of the H-O_{2c} increases to 1.961Å from 1.793 Å in 2Ni-TiO_2. The large charge transfer and geometrical changes on the surface may be associated with the release of the large amount of energy from the formation of the stable complex 2H-O_{2c}-2Ni-TiO_2(a), 94.8 kcal/mol, in the H_2(g) + 2Ni-TiO_2 reaction.

As shown in Figure S9(f), one H atom adsorbed on an O_{2c} site and another H atom bonding with an O_{sub2} site in the bulk, the charge of 2 Ni atoms have been reduced by 0.1*e* while those of O_{2c} and O_{sub2} are increased by 0.24*e* comparing to those 2Ni-TiO_2. The charges of both H atoms are observed to be 0.6*e*.

As shown in Figure S9(g) and S9(h), the two H atoms get incorporated interstitially producing two OH groups at O_{sub1} and O_{sub3} sites in different regions of the subsurface of 2Ni-TiO_2. We observe significant atomic charge changes in the neighboring oxygen atoms inside the bulk. The charge of the subsurface oxygen is −1.03 *e*, whereas the charges of the two oxygens associating with 2H become -1.26 *e* and -1.20 *e* as shown in Figure S9(g) and -1.14*e* and -1.21*e* in Figure S9 (h). The charges of H atoms in both cases are around 0.7*e* and 0.6*e*. Here we have not observed a significant change in the charges of neighboring Ti atoms. The charges of one H atom at a surface O_{2c} and one in the bulk of 2Ni-TiO_2 are shown in Figures S9 (j) and (k). We have also carried out the Bader charge analysis for the O being reduced to H_2O in 2Ni-TiO_2 (Figure S9(i)); the result shows that the charge of the O in H_2O inside the bulk is -1.30*e*, while those of the 2 H are 0.64*e* and 0.70*e*. Here we also did not note any significant change in the charges of Ni's neighboring Ti atoms. These results clearly show that the new localized states appearing between the VB and CB due to the H_2O formation in the subsurface, H_2O-2Ni(b), derive primarily from the contributions of the Ni and its neighboring O atoms. The contribution from Ti3d is significantly lower comparing with those of Ni and O.

Conclusions

To summarize, we have studied the effect of Ni-doping in TiO_2 nanoparticles (NPs) experimentally and computationally on the hydrogenation process. Experimentally, we have found that TiO_2 NPs of approximately 20 nm in diameter doping with a small amount of Ni prepared by a sol gel method can be readily

hydrogenated at T<623K under near atmospheric pressure condition. The hydrogenated black NP films exhibit a very broad UV-Vis absorption extending well beyond 800 nm. The black NPs also show a high efficiency for photo-catalytic water splitting (using 10% ethanol as a sacrificial agent) according to our preliminary test. The mechanism for the hydrogenation process on Ni-doped TiO_2 has also been investigated by quantum-chemical calculations. The result indicates that the presence of 1 Ni atom on the surface of a 24-unit [TiO_2] cell, representing approximately 4% dopant, can reduce the barrier for the dissociative adsorption of H_2 by as much as ~40 kcal/mol with a significant enhancement in H-atom generation and migration into the bulk. The predicted density of states of the hydrogenated Ni-TiO_2 NPs also reveal the presence of prominent impurity states in the band-gap when H or its reaction product, H_2O, is present in the bulk. Furthermore, the theoretical result also indicates that the enthalpies of hydrogenation reactions producing the reduced H- and H_2O-species on the surface or inside the bulk increase by as much as 80 kcal/mol because of the presence of the Ni-dopant.

Notes and references

1 T. Leshuk, R. Parviz, P. Everett, H. Krishnakumar, R. A. Varin, and F. Gu, *ACS Applied Materials & Interface.,* 2013, ***5***, 1892-1895.

2 Y. Yan, M. Han, A. Konkin, T. Koppe, D. Wang, T. Andreu, G. Chen, U. Vetter, J. R. Morante, P. Schaaf, *J. Mater. Chem. A.*, 2014, **2**, 12708-12716.

3 X. Chen, L. Liu, P. Y. Yu, S. S. Mao, *Science.*, 2011, **331**, 746-750.

4 G. Wang, H. Wang, Y. Ling, Y. Tang, X. Yang, R. C. Fitzmorris, C.Wang, J. Z. Zhang, and Y. Li, *Nano. Lett.*, 2011, **11**, 3026-3033.

5 Z. Zheng, B. Huang, J. Lu, Z. Wang, X. Qin, X. Zhang, Y. Dai, and M. H. Whangbo, *Chem. Commun.*, 2012, **48**, 5733-5735.

6 Y. H. Hu, *Angew. Chem. Int. Ed.*, 2012, **51**, 12410-12412.

7 C. Sun, Y. Jia, X. H. Yang, H. G. Yang, X. Yao, G. Q. Lu, A. Selloni, S. C. Smith, *J. Phys. Chem. C.*, 2011, **115**, 25590-25594.

8 A. Naldoni, M. Allieta, S. Santangelo, M. Marelli, F. Fabbri, S. Cappelli, C. L. Bianchi, R. Psaro, V. D. Santo, *J. Am. Chem. Soc.*, 2012, **134**, 7600-7603.

9 P. Raghunath, W. F. Huang, M. C. Lin, *J. Chem. Phys.*, 2013, **138**, 154705.

10 S. Primdahl, M. Mogensen, *J. Electrochem. Soc.*, 1997, **144**, 3409-3419.

11 P. Holtappels, I. C. Vinke, L. G. J. de Haart, U. Stimming, *J. Electrochem. Soc.,* 1999, **146**, 1620-1625.

12 (a) M. H. weng, H. T. Chen, Y. C. Wang, S. P. Ju, J. G. Chang, M. C. Lin, *Langmuir.*, 2012, **28**, 5596-5605; (b) Z. Cheng, J. H. Wang, Y. M. Choi, L. Yang, M. C. Lin, M. Liu, *Energy Environ. Sci.*, 2011, **4**, 4380-4409.

13 A. Faes, A. Hessler-Wyser, A. Zryd, J. V. Herle, *Membranes*, 2012, **2**, 585-664.

14 (a) M. Z. Selcuk, M. S. Boroglu, I. Boz, *Reac. Kinet. Mech. Cat.*, 2012, **106,** 313-324; (b) T. sun, J. Fan, E. Liu, L. Liu, Y. Wang, H. Dai, Y. Yang, W. Hou, X. Hu, Z. Jiang, *Powder Technology*, 2012, **228**, 210-218.

15 See ESI†

16 (a) G. Kresse, J. Furthmüller, *Phys. Rev. B.,* 1996, **54**, 11169; (b) G. Kresse, J. Hafner, *Phys. Rev. B*., 1993, **47**, 558.

17 S. L. Dudarev, G. A. Botton, S. Y. Savrasov, C. J. Humphreys, A. P. Sutton, *Phys. Rev. B.*, 1998, **57**, 1505-1509.

18 (a) C. Lee, W. Yang, R. G. Parr, *Phys. Rev. B.,* 1988, **37**, 785; (b) J. P. Perdew, K. Burke, M. Ernzerhof, *Phys. Rev. Lett*., 1996, **77**, 3865-3868.

19 J. K. Burdett, T. Hughbanks, G. J. Miller, J. W. Richardson, J. V. Smith, *J. Am. Chem. Soc.*, 1987, **109**, 3639-3646.

20 G. Henkelman, B. P. Uberuaga, H. Jónsson, *J. Chem. Phys.*, 2000, **113**, 9901.

21 E. Finazzi, C. Di Valentin, G. Pacchioni, A. Selloni, *J. Chem. Phys.*, 2008, **129**, 154113.

22 M. J. Han, T. Ozaki, J. Yu, *Phys. Rev. B.*, 2006, **73**, 045110.

23 (a) D. V. Bavykin, A. A. Lapkin, P. K. Plucinski, J. M. Friedrich, F. C. Walsh, *J. Phys. Chem. B.*, 2005, **109***,* 19422-19427; (b) S. H. Lim, J. Luo, Z. Zhong, W. Ji, J. Lin, *Inorg. Chem.*, 2005, **44***,* 4124-4126.

24 (a) M. M. Islam, M. Calatayud, G. Pacchioni, *J. Phys. Chem. C.*, 2011, **115***,* 6809-6814; (b) F. Lin, G. Zhou, Z. Li, J. Li, J. Wu, W. Duan, *Chem. Phys. Lett.*, 2009, **475**, 82-85.

† Electronic supplementary information (ESI) available.

Acknowledgement: The authors acknowledge the supports from the ATU Plan of the Ministry of Education, Taiwan, and also from the National Center for High-performance Computing for providing the computer time. MCL thanks the Ministry of Education of Taiwan for the distinguished visiting professorship at NCTU.

Table 1. Band gaps of Ni doped TiO_2

Sample	Absorption edge /nm	Band gap /eV
TiO_2	380.4	3.26
1.0% $NiTiO_2$	392.0	3.16
3.4% $NiTiO_2$	406.1	3.05
5.0% $NiTiO_2$	416.6	2.98
7.5% $NiTiO_2$	410.0	3.02

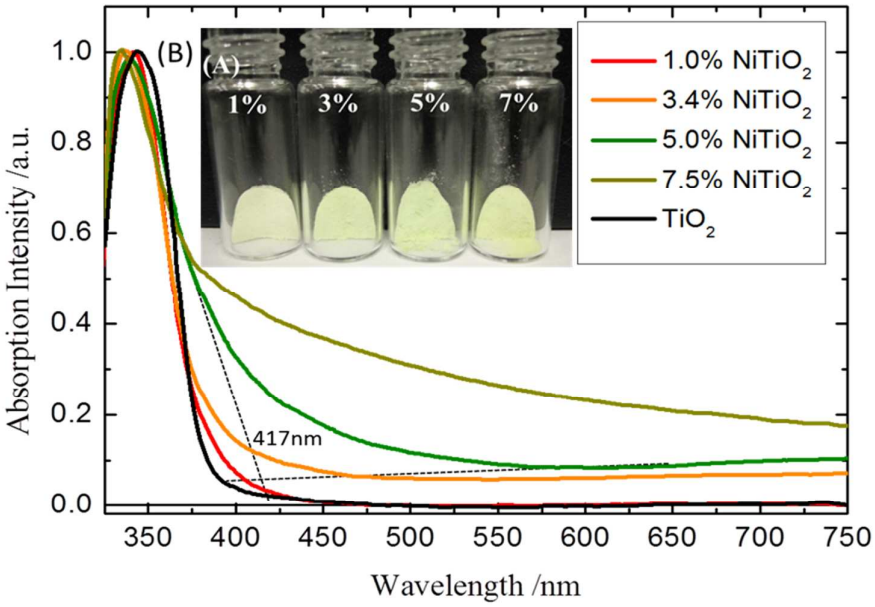

Figure 1. (A) The picture of Ni doped TiO_2 powders and (B) The UV-Vis absorption spectra of Ni doped TiO_2 thin film.

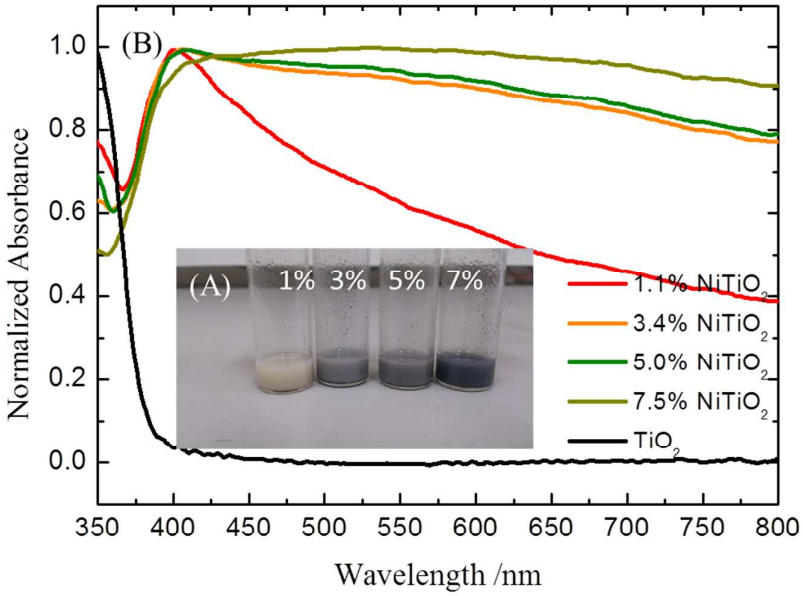

Figure 2. (A) The picture of hydrogenated Ni-TiO_2 methanol mixture and (B) The UV-Vis absorption spectra of hydrogenated Ni-TiO_2 thin film

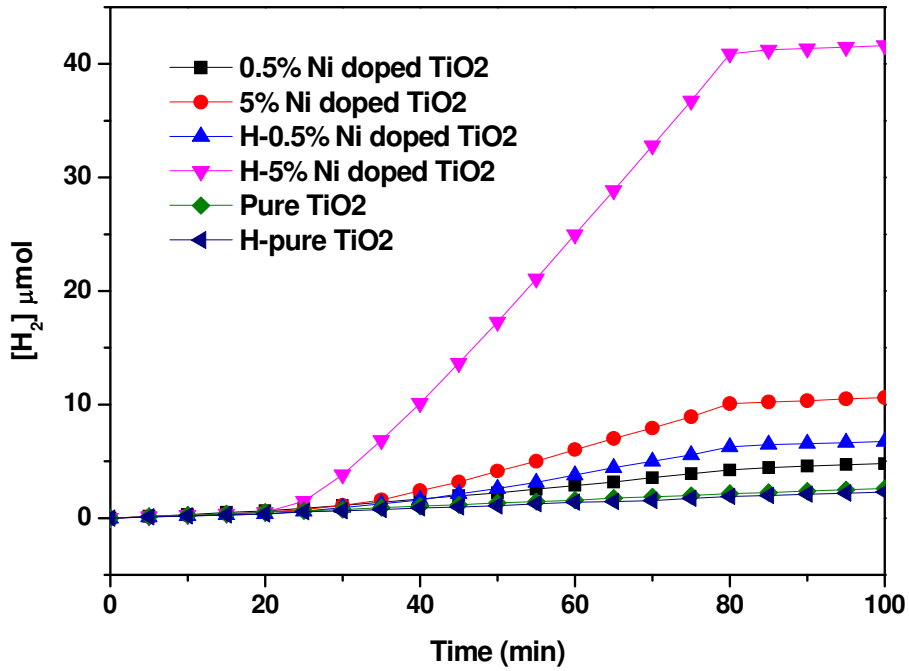

Figure 3. Hydrogen production rates under 1-hr illumination of NPs with about 2 W Xe-lamp output using 10% ethanol as sacrificial agent (light on: time 20~80 min). The relative efficiencies of pure TiO_2, hydrogenated TiO_2, 5% Ni-doped TiO_2 and hydrogenated Ni-doped TiO_2 with 5% Ni-doping are 1:1:4:18.

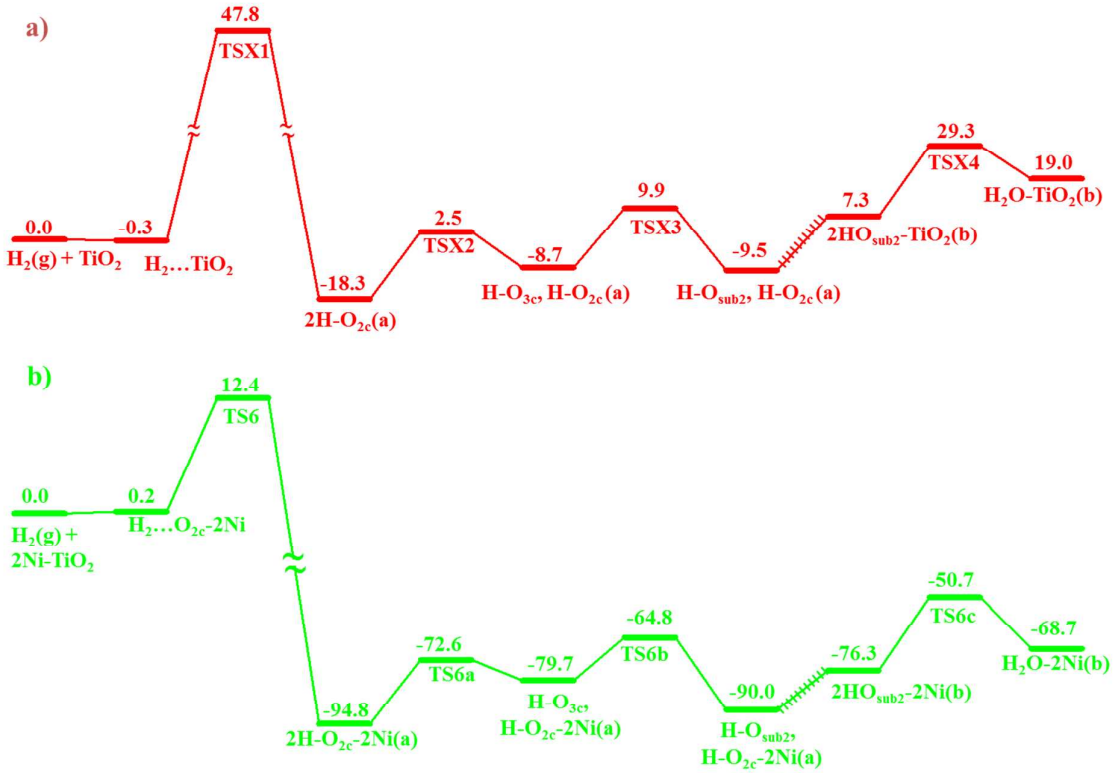

Figure 4. Predicted potential energy diagrams for (a) H_2 dissociation on the $TiO_2(101)$ surface and b) H_2 dissociation on the $2Ni\text{-}TiO_2(101)$ surface with the DFT + U method. The corresponding geometries are shown in Figure S5-S6. The hashed lines show omission of several small barriers in both energy profiles.

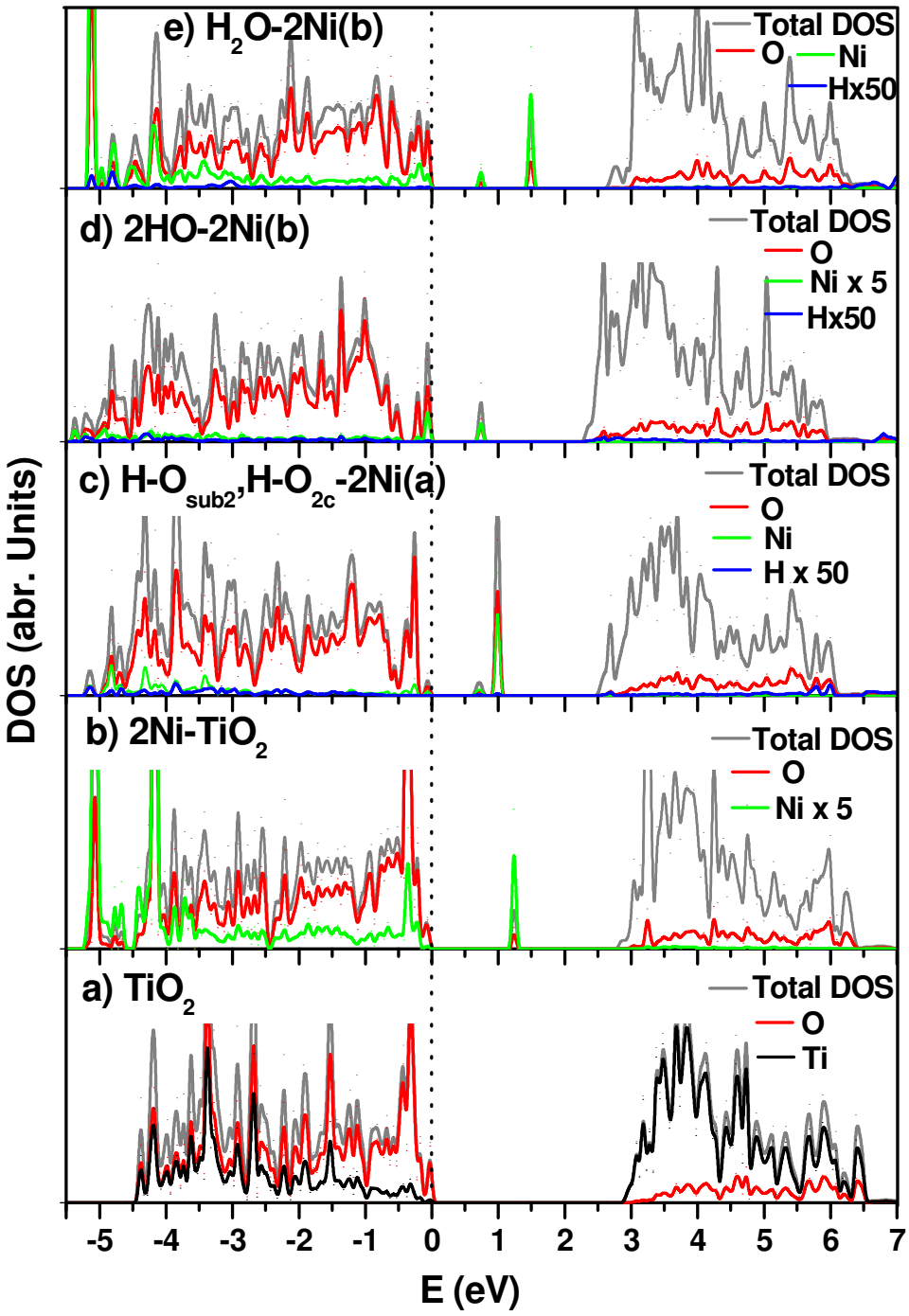

Figure 5. Density of states (DOS) for a) clean TiO_2, b) two Ni doped TiO_2, c) one H on the surface and one H inside the bulk of 2Ni doped TiO_2, (d) 2H inside the bulk of 2 Ni doped TiO_2 and (e) H_2O formed inside the bulk of 2 Ni doped TiO_2 calculated at the DFT + U level (U = 4.0 eV for Ni and Ti) (for clarity, H and Ni PDOS peaks are magnified). Their optimized geometries are shown in Figure S4 and S5. The dashed vertical line represents the position of the Fermi level.

Graphical Abstract

The hydrogenated black Ni-TiO_2 nanoparticles exhibit a much greater efficiency in water splitting producing H_2 gas over those of non-hydrogenated TiO_2 and Ni-doped TiO_2.